PNAS RESEARCH ARTICLE | IMMUNOLOGY AND INFLAMMATION

Cryo-EM structure of the human chemerin receptor 1–Gi protein complex bound to the C-terminal nonapeptide of chemerin

Junlin Wang[a,1], Geng Chen[a,1], Qiwen Liao[a,1], Wenping Lyu[b], Aijun Liu[a,c], Lizhe Zhu[b], Yang Du[a,2], and Richard D. Ye[a,2]

Edited by H. Eric Xu, Shanghai Institute of Materia Medica Chinese Academy of Sciences, Shanghai, China; received August 26, 2022; accepted January 27, 2023 by Editorial Board Member Nieng Yan

Chemerin is a processed protein that acts on G protein-coupled receptors (GPCRs) for its chemotactic and adipokine activities. The biologically active chemerin (chemerin 21-157) results from proteolytic cleavage of prochemerin and uses its C-terminal peptide containing the sequence YFPGQFAFS for receptor activation. Here we report a high-resolution cryo-electron microscopy (cryo-EM) structure of human chemerin receptor 1 (CMKLR1) bound to the C-terminal nonapeptide of chemokine (C9) in complex with Gi proteins. C9 inserts its C terminus into the binding pocket and is stabilized through hydrophobic interactions involving its Y1, F2, F6, and F8, as well as polar interactions between G4, S9, and several amino acids lining the binding pocket of CMKLR1. Microsecond scale molecular dynamics simulations support a balanced force distribution across the whole ligand–receptor interface that enhances thermodynamic stability of the captured binding pose of C9. The C9 interaction with CMKLR1 is drastically different from chemokine recognition by chemokine receptors, which follow a two-site two-step model. In contrast, C9 takes an "S"-shaped pose in the binding pocket of CMKLR1 much like angiotensin II in the AT1 receptor. Our mutagenesis and functional analyses confirmed the cryo-EM structure and key residues in the binding pocket for these interactions. Our findings provide a structural basis for chemerin recognition by CMKLR1 for the established chemotactic and adipokine activities.

GPCRs | chemerin | adipokine | innate immunity | cryo-EM

Significance

Chemerin is a protein with chemotactic activity, but how it interacts with the cognate receptors remains unclear and the chemerin–receptor complex was unstable for structural analysis. We took advantage of the C-terminal nonapeptide (C9), which displays full agonistic activity of chemerin, and solved the cryo-electron microscopy (cryo-EM) structure of the chemokine-like receptor 1 (CMKLR1) bound to C9 and in complex with Gi proteins. C9 assumes an "S"-shaped pose in the binding pocket which is very different from chemokine binding to chemokine receptors but similar to the binding mode of angiotensin II to AT1 receptor. These findings provide the structural basis for ligand recognition by CMKLR1 and G protein activation for its chemotactic and adipokine activities.

Chemerin is a protein encoded by the *retinoic acid receptor responder 2* gene, also termed tazarotene-induced gene (1, 2). A processed chemerin with removal of its signal peptide and C-terminal 6 amino acids acquires chemotactic activity and is a natural ligand of chemerin receptor 1 (ChemR23, CMKLR1) (2, 3). Chemerin induces chemotaxis of immature dendritic cells and macrophages (2). Subsequent reports found a broader spectrum of chemotactic activities in cells that respond to chemerin, including myeloid cells and natural killer cells (4–6). There is a positive correlation between serum chemerin level and the expression of proinflammatory cytokines including TNFα, interleukin-6, and C-reactive protein (7, 8), suggesting that chemerin has proinflammatory properties. Besides its chemotactic activity, chemerin expression is closely associated with differentiation of adipocytes, and loss of chemerin expression abrogates adipogenesis (9). There is also a correlation between chemerin expression and obesity, indicating that chemerin is an adipokine (9–11). More recent studies have shown that the chemerin-CMKLR1 axis is involved in immunometabolism through interleukin-33 (IL-33) and type 2 innate immunity (12). The chemerin–CMKLR1 axis also plays a role in epithelial cells by restricting microbiota-driven colonic neutrophilia and tumorigenesis (13).

Although chemerin is known for its chemotactic activity, there are clear distinctions between chemerin and chemokines as chemokines have a core structure stabilized with disulfide bonds and a flexible N-terminal segment (14), features that are missing from chemerin. Pre-prochemerin is a 163-amino acid protein without chemotactic activity. Removal of the N-terminal signal peptide results in prochemerin (21-163) with low bioactivity. Proteolytic cleavage of the C-terminal prosegment (158-163) generates bioactive chemerin (21-157) with full chemotactic activity (15, 16). Processing of prochemerin by a variety of peptidases leads to protein fragments of various lengths and bioactivities (15). A study using synthetic peptides of the C-terminal fragments of chemerin found that removal of just one amino acid from chemerin results in a chemerin fragment (21-156) with less than 20% of the original activity. Moreover, the C-terminal 9 amino acids (C9, 149-157) retains full bioactivity of chemerin (21-157), indicating that it is the C terminus of the chemerin that harbors the structural determinants for

Author contributions: R.D.Y. designed research; J.W., G.C., and Q.L. performed research; A.L. and L.Z. contributed new reagents/analytic tools; G.C., Q.L., W.L., and A.L. analyzed data; and Y.D. and R.D.Y. wrote the paper.

The authors declare no competing interest.

This article is a PNAS Direct Submission. H.E.X. is a guest editor invited by the Editorial Board.

[1]J.W., G.C., and Q.L. contributed equally to this work.

[2]To whom correspondence may be addressed. Email: yangdu@cuhk.edu.cn or richardye@cuhk.edu.cn.

This article contains supporting information online at https://www.pnas.org/lookup/suppl/doi:10.1073/pnas.2214324120/-/DCSupplemental.

Published March 7, 2023.

receptor activation (17). Therefore, C9 has been widely used in in vitro studies for the characterization of chemerin receptors in functional assays.

CMKLR1 is a G protein-coupled receptor (GPCR) of the rhodopsin-like subfamily. CMKLR1, also termed ChemR23 (3), was initially identified as an orphan receptor with homology to several chemokine receptors (18). CMKLR1 has been found in hematopoietic tissues (18), adipocytes (9), endothelial cells (19), and vascular smooth muscle cells (20), correlating with its possible role in regulating leukocyte functions, obesity and cancer development. *GPR1* (21) is a gene coding for another chemerin receptor (22, 23). These two receptors share more than 80% of sequence homology, and both recognize C9 as an agonist, but they activate different signaling pathways (23). Given the growing interests in the diverse bioactivities of chemerin as well as the lack of significant sequence homology between chemerin and other GPCR ligands such as chemokines, it is important to understand how chemerin activates the cognate receptors. In the present study, we employed cryo-electron microscopy (cryo-EM) to determine the structure of CMKLR1 bound to C9 and complexed with heterotrimeric Gi proteins. Our results identified structural features that differ from known chemokine receptors in the recognition of chemotactic proteins.

Results and Discussion

Cryo-EM Structure of the CMKLR1-Gi Complex. The CMKLR1-Gi-scFv16 complex bound to the chemerin nonapeptide C9 (^{149}YFPGQFAFS^{157}) was prepared (*SI Appendix*, Figs. S1 and S2) and its structure was determined by cryo-EM to an overall resolution of 2.8 Å (Fig. 1 *A* and *B*). The antibody fragment scFv16 (24) was used for stabilization of the C9-CMKLR1-Gi protein complex. The ligand-binding pocket of CMKLR1 was surrounded by transmembrane (TM) helices 2, 3, 4, 5 and the second extracellular loop (ECL2), with minor involvement of TM6, 7 and ECL1 (Fig. 1*A*). The C9 peptide assumes a pose with its C terminus inserted deep into the binding pocket (Fig. 1*B*). In this structural model (Fig. 1 *C*–*E*), the N-terminal Y1 and F2 interacts with the aromatic side chains of F190^{ECL2}, F294$^{7.31}$, and H268$^{6.61}$ [superscripts indicate the Ballesteros–Weinstein numbering scheme (25)]. G4 in the peptide backbone formed polar interactions with E283$^{6.58}$ and R178$^{4.64}$, possibly providing an anchor for the C9 peptide to adopt an "S"-shaped conformation for receptor activation. The C-terminal part of the C9 peptide including F6 and F8 forms extensive hydrophobic interactions with Y103^{ECL1}, F295$^{7.32}$ (F6), and L119$^{3.32}$, M123$^{3.36}$, Y276$^{6.51}$, and I306$^{7.43}$ (F8) that serve to stabilize the peptide ligand in the

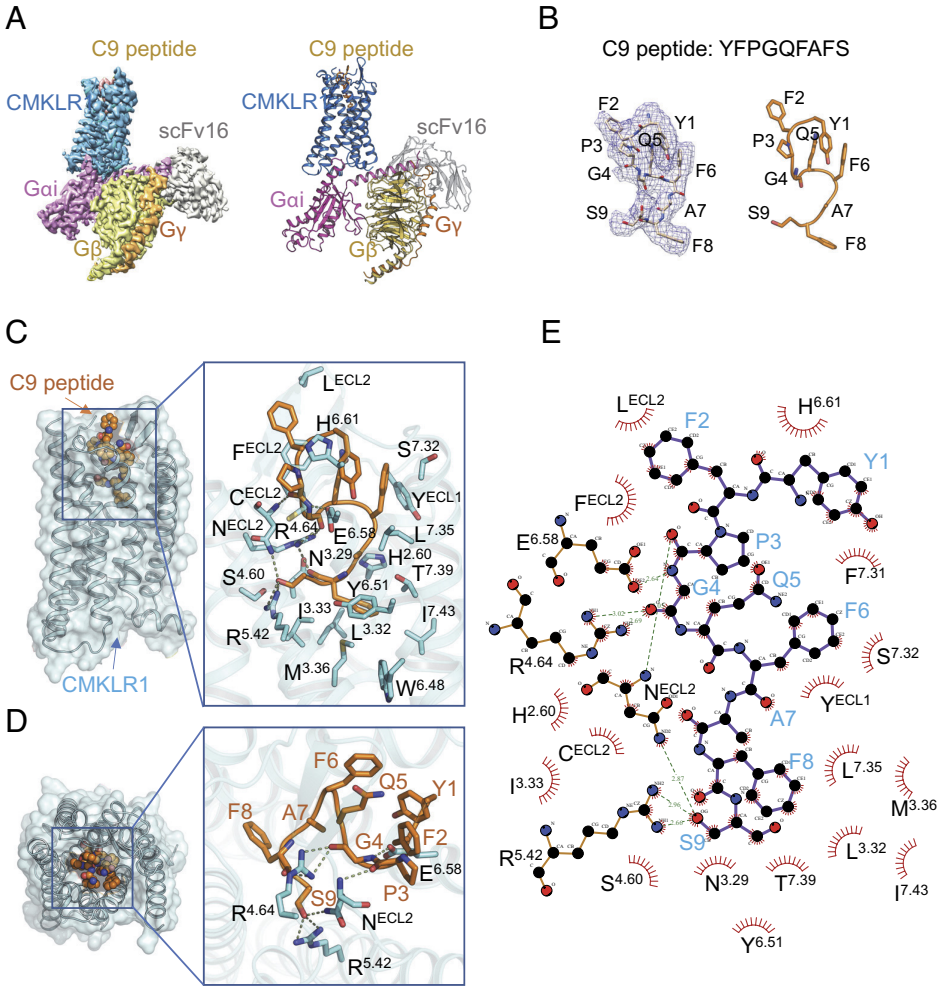

Fig. 1. Overall structure and ligand-binding pocket of C9-CMKLR1-Gi complex. (*A*) Cryo-EM density map (*Left*) and structural model (*Right*) of the CMKLR1-Gi-scFv16 complex bound to C9 in side view. (*B*) Cryo-EM density map and the peptide backbone of C9. (*C*) Overall structure of CMKLR1-C9 complex from side view (*Left*) and key interaction residues (*Inset* at *Right*). In the overall structure, the receptor (cyan) is shown in cartoon and surface representation. The C9 peptide is shown in sphere with carbon in orange. The residues of CMKLR1 within 4 Å from the C9 peptide (orange licorice and ribbon) are shown in cyan licorice. The hydrogen bonds are displayed as dashed lines. (*D*) Extracellular view of the overall structure (*Left*) and polar interactions (*Inset* at *Right*) of the CMKLR1-C9 complex. The residue numbering of CMKLR1 follows the Ballesteros–Weinstein nomenclature. (*E*) Schematic representation of interactions between CMKLR1 and C9 analyzed By LigPlot+ program. The stick drawings of CMKLR1 and C9 are shown as orange and blue sticks, respectively.

binding pocket. At the C-terminal end, S9 forms a hydrogen bond with R224$^{5.42}$, which is an amino acid conserved in several GPCRs for chemotactic peptides such as FPR1 and FPR2 (26–29). F8 inserts deep into the binding pocket, just above the "toggle switch" W273$^{6.48}$.

Thermodynamic Stability of CMKLR1-C9 Interface. Five independent 1-μs-long full-atom molecular dynamics (MD) simulations were performed at room temperature. The results demonstrated that the CMKLR1-C9 interface captured by Cryo-EM is overall stable under thermodynamic perturbation, and the "S"-shaped pose of C9 peptide is well kept through the entire 5-μs trajectory (Fig. 2*A*). Among the peptide–protein contacts observed by cryo-EM (Fig. 1 *C–E*), the N terminus of C9 is stabilized largely by π–π stacking between Y1 and F294$^{7.31}$ and between F2 and F190^{ECL2} (Fig. 2*B*). Not observed in the cryo-EM structure but identified in the MD simulations are the two hydrogen bonds between Y1 and E283$^{6.58}$ of the receptor (Fig. 2*C*). The π–π stacking and hydrogen bond between Y1 and the ligand binding pocket are consistent with the reduced activity (~30%) in functional assays when Y1 was missing or substituted by alanine (17). At the C terminus of the peptide ligand, S9 was locked mainly by electrostatic interactions including a salt bridge with R224$^{5.42}$ and a hydrogen bond with Y276$^{6.51}$ (Fig. 2*C*). In addition, hydrophobic interactions play a crucial role in the binding of C9, with F8 inserting into a hydrophobic cavity formed by F88$^{2.53}$, L92$^{2.57}$, L119$^{3.32}$, M123$^{3.36}$, Y276$^{6.51}$, and I306$^{7.43}$ (Fig. 2*B*). These interactions were also in line with a previous report showing that removal of F8 and S9 or alanine substitution of F8 markedly reduced the bioactivity of C9 (17). In comparison, the hydrophobic (Y103^{ECL1}, L298$^{7.35}$ in Fig. 2*B*) and hydrophilic (C189^{ECL2}, N191^{ECL2}, E283$^{6.58}$ in Fig. 2*C*) interactions of the receptor with the middle core of C9 (P3-G4-Q5-F6) are well separated in the horizontal direction, applying a "shear force" to the middle core of C9 normal to the radial direction. Overall, we confirmed that the thermodynamically stable "S"-shaped conformation of C9 in complex with CMKLR1 is a result of balanced force distribution across the whole ligand–receptor interface.

Functional Analysis of the CMKLR1-C9 Interaction. Following CMKLR1 structural analysis, site-directed mutagenesis of the receptor was conducted to confirm the functional interaction between key residues in C9 and the CMKLR1 binding pocket. Alanine substitutions of the predicted key amino acids in the binding pocket were followed by functional analysis of the mutants in G protein dissociation assay that measures CMKLR1 activation, and in intracellular cAMP concentration reduction assay that is a function of activated Gαi proteins (Fig. 3). The results of these assays are highly consistent. The alanine substitution of R178$^{4.64}$, which is conserved among several Class A GPCRs such as C3aR and C5aR, led to a drastic decrease in C9-induced G protein dissociation and cAMP concentration reduction (Fig. 3). Likewise, alanine substitution of another polar residue, E283$^{6.58}$, resulted in decreased potency of C9-induced G protein dissociation by approximately three orders of magnitude based on EC_{50} (Fig. 3). These results support the predicted role of the substituted amino acids in hydrogen bond formation with G4 and Y1 (Fig. 3*B*). Substitution of R224$^{5.42}$, which is predicted to form a salt bridge with S9 and is also conserved among such receptors as FPR1 and FPR2, led to a decreased potency by two orders of magnitude in G protein dissociation and cAMP concentration reduction assays based on EC_{50} values.

In addition to polar interactions, hydrophobic interactions play an important role in C9 interaction with CMKLR1. F8 is predicted to interact with the hydrophobic side chain of Y276$^{6.51}$ that in turn may influence the nearby "toggle switch" (W273$^{6.48}$). However, alanine substitution of these amino acids led to poor expression of the resulting receptors (*SI Appendix*, Fig. S3), suggesting that an intact hydrophobic cavity in the bottom of the binding pocket (Fig. 3*A*) is critical to the overall structure of CMKLR1. Alanine substitution of H95$^{2.60}$, N116$^{3.29}$, and S295$^{7.32}$, which are within 4.5 Å to C9, also had a negative impact

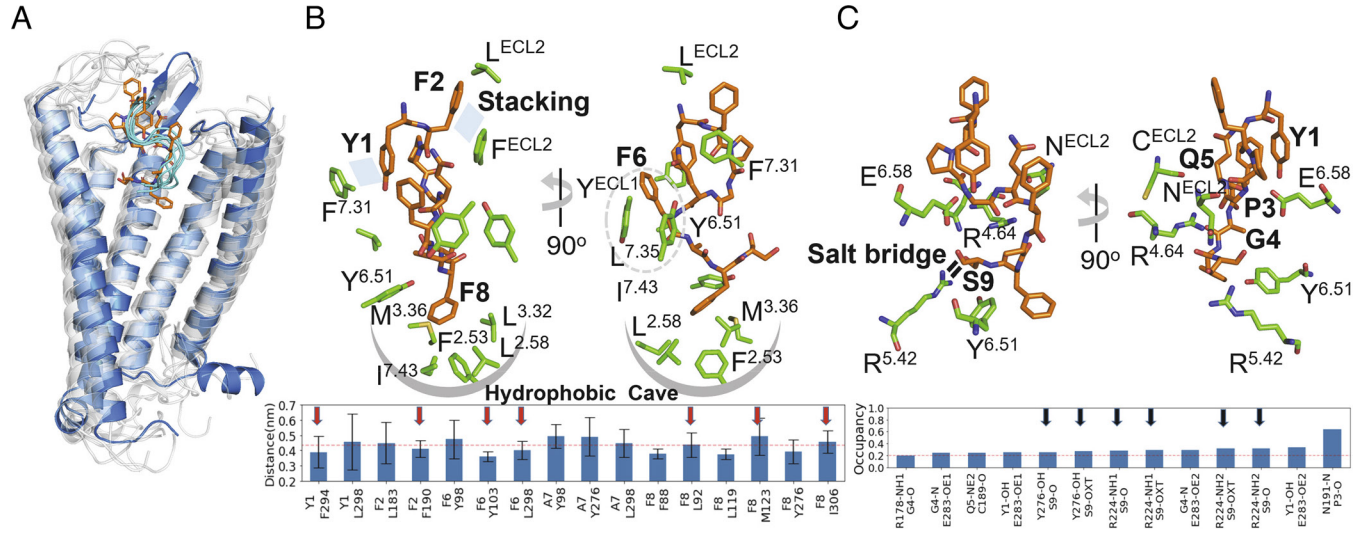

Fig. 2. Thermodynamic stability analysis of the CMKLR1-C9 interface with microsecond scale MD simulations. (*A*) Superimposed representative conformations (grey) obtained from MD simulations to the experimental structure (blue). The "S" shape of C9 backbone is rendered in carton representation (cyan). Side chain orientation of C9 is displayed for experimental structure only (orange). (*B*) Hydrophobic interaction between CMKLR1 and C9. The overall distribution of major hydrophobic residues (green) relative to the C9 (orange) in structure is shown in the upper left panel; major pair-wise stacking interactions and the hydrophobic cave for F8 side chain embedding are highlighted in crescent shape. The contacts with residue-residue distance (closest heavy atom) below the average value (red dotted line) of all hydrophobic contacts are considered as major contacts (marked by red arrows, *Bottom* panel). (*C*) Hydrogen bond contacts of CMKLR1 to C9. The overall distribution of major hydrogen bond involving residues (green) relative to the C9 (orange) in structure is shown in the *upper left* panel; the major hydrogen bond interactions and the salt bridge between S9 and R224 are highlighted in bold lines. Here, the hydrogen bonds with occupancy greater than the average value (red dotted line) of all hydrogen bonds are considered as major hydrogen bond contacts (*Bottom*). The hydrogen bonds formed with S9 are marked with black arrows.

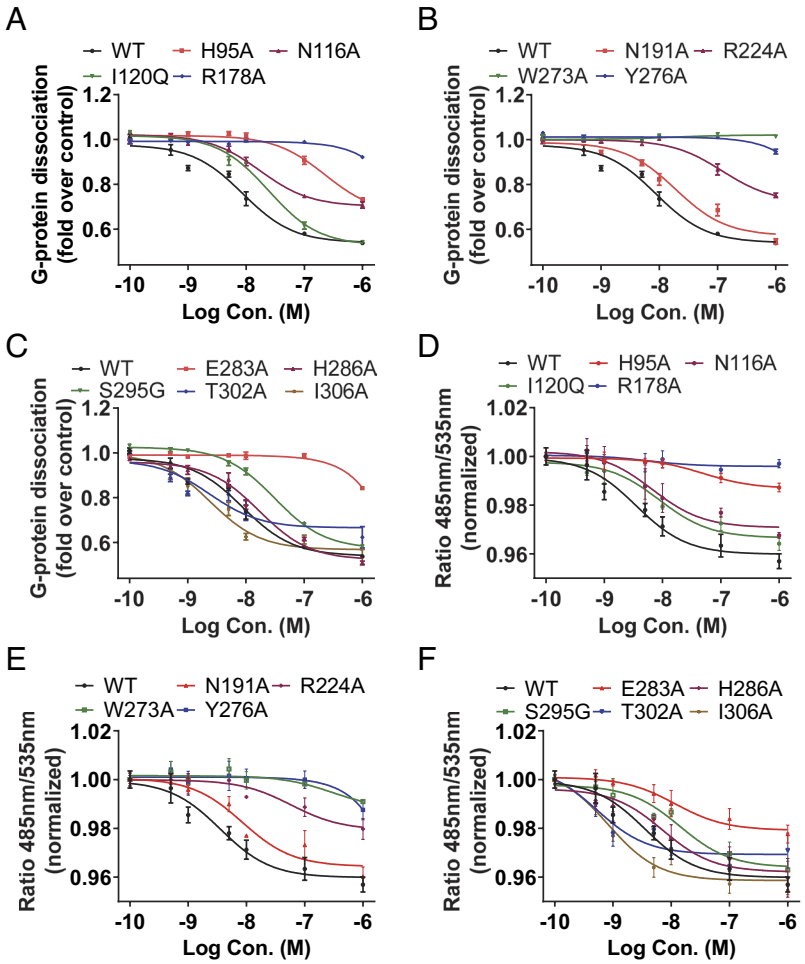

Fig. 3. G protein dissociation, cAMP concentration reduction. (*A–C*) G protein dissociation in HEK293T cells cotransfected to express WT or mutant CMKLR1, Gαi1-LgBiT, Gβ1, and SmBiT-Gγ2. Coelenterazine H was added to 10 μM and baseline was determined after 2 h of incubation. C9-induced luminescent signals were measured 15 min after ligand addition and divided by the baseline count. The fold changes were further normalized to PBS-treated cells. (*D–F*) cAMP concentration inhibition in HEK293T cells, co-transfected to express WT or mutant CMKLR1 and mTurquoise2-Epac SH187-cp73venus. Forty-eight hours after transfection, C9 was added for 30 min, and then forskolin (3 μM, 37 °C, 30 min), intracellular cAMP levels were measured and expressed as FRET ratio of emissions at 485 nm over 535 nm. All data shown are means ± SEM from three independent experiments.

on CMKLR1 activation (Fig. 3). Taken together, site-directed mutagenesis combined with functional assays support the cryo-EM structural model of C9-bound CMKLR1.

Activation Mechanism of CMKLR1. Since a solved structure of an inactive CMKLR1 was unavailable, the structure of an antagonist-bound C5aR (C5aR-PMX53, PDB ID:6C1R) was used for identification of conformational changes associated with the activation of CMKLR1. With an overall sequence identity of 35.8%, C5aR is one of the most homologous GPCRs to CMKLR1. In C9-bound CMKLR1, the receptor showed a conformation rearrangement involving outward movement of TM6 and inward shift of TM7 relative to the transmembrane helices of the inactive C5aR (Fig. 4*A*). Like other Class A GPCRs, a conserved hydrogen bond was found between R137$^{3.50}$ and Y240$^{5.58}$ in the C9-bound CMKLR1, but it was absent in the inactive C5aR structure (Fig. 4*B*). Moreover, the P232$^{5.50}$-I/V127$^{3.40}$-F269$^{6.44}$ motif displayed rotamer conformational changes in the C9-bound CMKLR1 structure relative to the inactive C5aR structure (Fig. 4*C*). The highly conserved residue W273$^{6.48}$, representing the "toggle switch," showed an "anticlockwise" rotation in the C9-bound CMKLR1 (Fig. 4*D*), consistent with the conformational rearrangement of the "toggle switch" upon GPCR activation (30, 31).

The interaction of an activated CMKLR1 with the Gi class of heterotrimeric G proteins was next investigated. Binding of C-terminal nonapeptide (C9) to CMKLR1 can activate the three Gαi subtypes (Gαi1, Gαi2 and Gαi3) and the two Gαo isoforms (Gαoa and Gαob). Among these G proteins, The Gαi1 shows relatively high binding affinity toward CMKLR1 (32) and was chosen for this study. DNGαi1, a dominant negative form of human Gαi1 that incorporates the G203A and A326S mutations, was adopted for its decreased affinity for nucleotide binding and increased stability for Gαβγ complex formation (33, 34) and was cloned into the pFastBac vector. The N-terminal 6×His-tagged Gβ1 and Gγ2 were cloned into the pFastBac-Dual vector for coexpression. The three types of baculoviruses (CMKLR1, DNGαi1, Gβ1γ2) were cotransfected into Sf9 insect cells at the ratio of 1:4:2. In this structure, the α5 helix of Gαi formed hydrophobic interactions with the intracellular loops of CMKLR1 involving I344, L348, and L353 of the α5 helix and V141$^{3.54}$, L247$^{5.65}$, L252^{ICL3}, I261$^{6.36}$, and I262$^{6.37}$ of CMKLR1 (Fig. 4*E*). Polar interactions were observed between N347, D350, C351, and G352 of Gαi and the carbonyl and side chains of S140$^{3.53}$, N74$^{2.39}$, R137$^{3.50}$, and K257$^{6.32}$ of CMKLR1, respectively (Fig. 4*E*). Interestingly, a hydrogen bond was found between K327 of H8 in CMKLR1 and D312 of the Gβ subunit, indicating a direct interaction between H8 of CMKLR1 and the Gβ subunit (Fig. 4*F*). Site-directed mutagenesis was conducted with alanine substitution of these amino acids in CMKLR1. The resulting mutants of CMKLR1 were individually expressed for functional

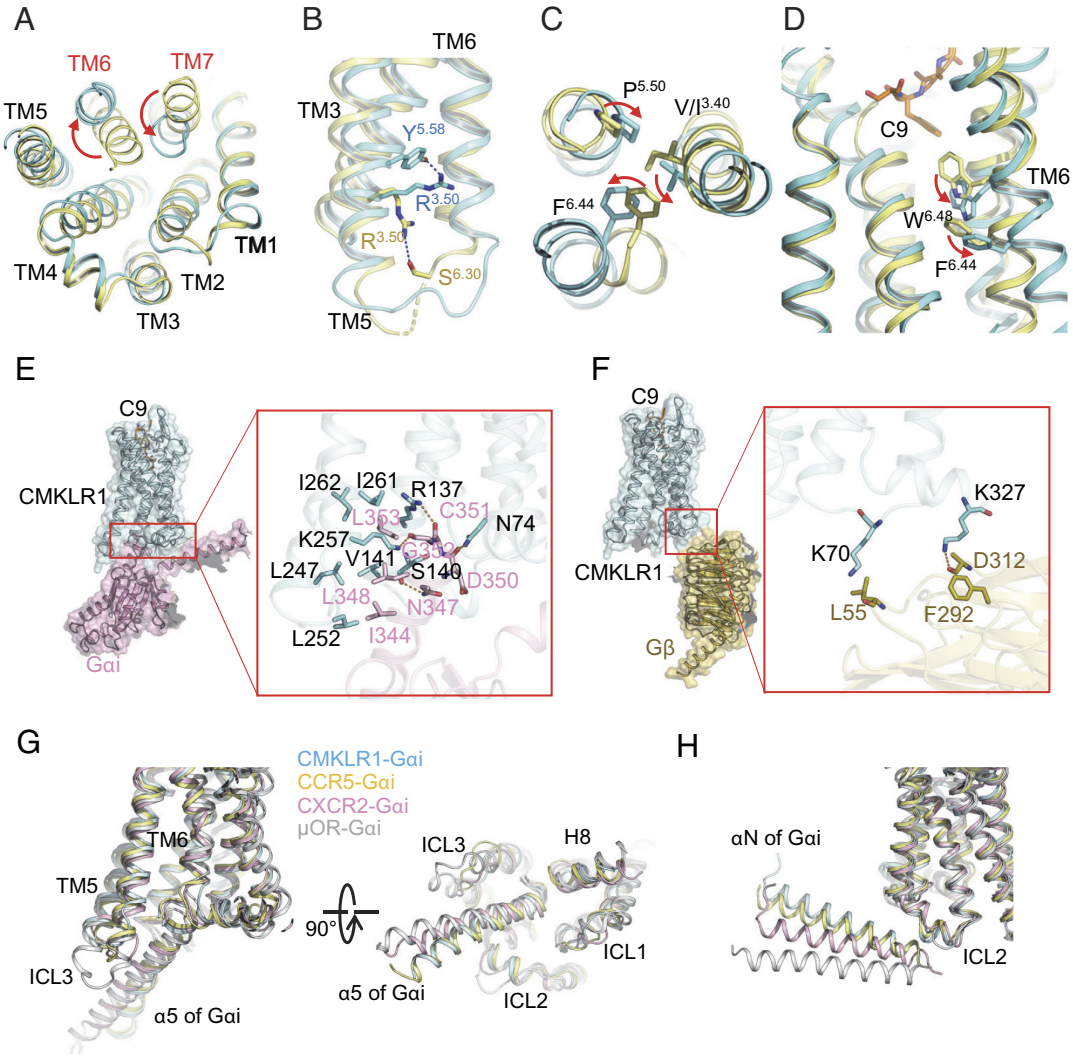

Fig. 4. Potential activation mechanism of the C9-bound CMKLR1-Gi complex. (*A*) Intracellular view of the movement of helix 6 and helix 7. The transmembrane helices in the superimposed structures of CMKLR1-C9 (cyan) and C5aR-PMX53 (yellow, PDB ID: 6C1R) are shown in cartoon representation. Red arrows indicate the direction of movement of helix 6 and helix 7 in the structures of CMKLR1-C9 (active) relative to C5aR-PMX53 (inactive). (*B*) Same as in (*A*) but the hydrogen bond between R137$^{3.50}$ and Y240$^{5.58}$ in CMKLR1 (blue) is compared with the C5aR residues R134$^{3.50}$ and S237$^{6.30}$ (yellow) that formed polar interactions (dashed lines). (*C*) The conformational change of the P232$^{5.50}$V/I127$^{3.40}$F269$^{6.44}$ triad. The residues at positions 3.40, 5.50, and 6.44 (Ballesteros-Weinstein nomenclature) in the structures of CMKLR1-C9 (cyan) and C5aR (yellow) are shown as licorice. (*D*) The conformational change of F269$^{6.44}$ and W273$^{6.48}$ in the C9-bound CMKLR1-Gi structure (cyan). Red arrows indicate the relocations of these residues relative to the inactive C5aR structure. (*E* and *F*) show the interactions between the α5 helix of Gαi (pink) and CMKLR1 (cyan) in the cavity at ICL3, TM5, TM6, and TM7 regions (*E*), and the interactions between Gβ subunit (yellow) and H8 of the receptor (cyan) (*F*). The hydrogen bonds between the receptor and Gαi subunit are shown as orange dash lines, whereas the polar interactions between the receptor and Gβ subunit are represented by orange dash lines. (*G*) Comparisons of the interactions between the α5 helix of Gαi and TM5, TM6, and ICL3 of several Gi-coupled receptors including CMKLR1 (cyan), CXCR2 (pink, PDB ID: 6LFO), CCR5 (yellow, PDB ID: 7F1R) and μOR (grey, PDB ID: 6CMO). The panel in the right shows the locations of ICL2, ICL1, and H8. (*H*) Same as (*G*) but the interactions of the αN helix of Gαi with these receptors are compared.

confirmation of the interaction with G proteins based on the inhibition of cytoplasmic cAMP accumulation by the activated Gi protein. As shown in *SI Appendix*, Fig. S4, all but S140$^{3.53}$A produced inhibitory effects with the R137$^{3.50}$A and K327^{H8}A producing the most prominent inhibition when compared with the WT receptor. These findings are consistent with our prediction, based on the solved structure of the C9-CMKLR1-Gi complex, that the charged residues R137$^{3.50}$ and K327 in H8 are both critical to the interaction of CMKLR1 with the heterotrimeric Gi proteins used in this study.

The engagement of Gi proteins by CMKLR1 was compared with other Gi-coupled GPCRs including CXCR2, CCR5, and μOR. Among these GPCRs, there is a common core of interface between C-terminal α5 helix of the Gαi protein and TM3, TM5, and TM6 of CMKLR1. Even though the overall architecture of GPCR-Gi interface is conserved, there are some differences in the interacting residues and the Gi conformations. The orientation of the Gαi coupled to CMKLR1 is different from other class A GPCRs (35): Both TM5 and TM6 in CMKLR1 are approximately 1 to 2 helical turns shorter than those in CXCR2, CCR5, and μOR, rendering a less extensive ICL3 that is also farther away from the α4-β6 loop of Gαi (Fig. 4*G*). In Gαi-coupled CMKLR1, two hydrogen bonds are formed between N149^{ICL2} of CMKLR1 and residues R32 and D193 of Gαi in its αN helix, thereby changing the conformation of αN helix for closer proximity to ICL2 in CMKLR1 than in other GPCRs (Fig. 4*H*). These features are characteristic in the CMKLR1-Gi complex.

Comparison of Agonist Binding Modes of CMKLR1 and Structural Homologs. Several Class A GPCRs share homology with CMKLR1 to different degrees, but all bind peptides or small protein ligands. To determine the similarities and differences of these receptors in ligand recognition, the C9-bound CMKLR1 structure was

compared with the solved structures of fMLF-bound formyl peptide receptor 1 (FPR1), endogenous chemokine CCL15-bound CCR1, vMIP-II-bound CXCR4, Type 1 angiotensin II (AngII) receptor (AT1R), and alpha-melanocyte-stimulating hormone (α-MSH)-bound melanocortin 1 receptor (MC1R) (Fig. 5). The last two receptors were chosen because they bind peptide ligands similar to the chemerin-derived C9 peptide. Among the Gi-coupled class A GPCRs that display chemotatic activities, FPR1 (34.71%), and CXCR4 (26.65%) display high sequence identity with CMKLR1. FPR1 has a deep binding pocket that accommodates a very small tripeptide with full agonistic activity (26, 27). Peptides bearing N-formyl methionine (formyl peptides) interact with FPR1 with the N-terminal fMet reaching the bottom of the binding pockets, and the tripeptide interacts with the D106$^{3.33}$-R201$^{5.38}$-R205$^{5.42}$ triad for high affinity binding and receptor activation (26, 27). The extracellular loops of FPR1 play a little role in ligand binding. In contrast, chemokine receptors use extracellular loops extensively for interaction with the core of chemokines, while the N-terminal fragments insert into the ligand binding pockets as illustrated in CCL15-bound CCR1 and vMIP-II-bound CXCR4 (Fig. 5). These two chemokine receptors have binding cavity shallower than that of CMKLR1. A two-site mode of chemokine binding is widely used among chemokine receptors (36). CCR1 uses a three-site binding mode for chemokine recognition, with the N terminus of CCR1 binding to CCL15 core, the N terminus of CCL15 inserting into CCR1 cavity, and the 30s loop of CCL15 interacting with ECL2 and ECL3 of CCR1 (37). CMKLR1 binding of the chemerin C9 peptide differs from the above modes of receptor–ligand interactions. C9 is a processed fragment of prochemerin with full bioactivity of chemerin. As such, C9-CMKLR1 interaction does not require contact of the core structure as seen in chemokines. However, because the current study determines only the C9-bound CMKLR1-Gi complex, it remains unclear whether full-length chemerin employs multisite binding mode for its interaction with CMKLR1.

For the interaction of the peptide ligands with the binding cavities of these GPCRs, C9 has its C terminus inserted into the binding pocket (C terminus-in) whereas fMLF and other formyl peptides use the "N terminus-in" mode for interaction of the formyl group with the D106$^{3.33}$-R201$^{5.38}$-R205$^{5.42}$ triad. The binding pocket in FPR1 is deeper than the one in CMKLR1. As a result, binding of the tripeptide is stable with a dissociation constant in low nanomolar range (38). C9 interaction with the binding pocket of CMKLR1 involves a salt bridge between S9 of the ligand and R224$^{5.42}$ of the receptor, which is similar to fMLF interaction with R205$^{5.42}$. However, C9 is additionally stabilized with interactions including π–π stacking through the aromatic side chains of Y1 and F2 and hydrophobic interactions through F6 and F8, which are absent from the structures of fMLF-FPR1, CCL15-CCR1, and vMIP-II-CXCR4. Since the structure of full chemerin-bound CMKLR1 has not been solved, we do not know how full-length chemerin interacts with the receptor. However, it is obvious that inclusion of more amino acids N-terminal to the C9 peptide does not improve binding and potency, as the C9 peptide (149-157) is just as potent as its longer homolog (chemerin 139-157) and the full-length chemerin (21-157) (17).

Whereas CMKLR1 is the first reported GPCR with a bound chemotactic peptide in "S"-shaped pose, a number of peptide ligands have been found to take this pose in their cognate receptors. Type 1 angiotensin II (AngII) receptor (AT1R) plays an important role in blood pressure regulation. AngII (Asp-Arg-Val-Tyr-Ile-His-Pro-Phe) is different from C9 in composition and does not display chemotactic activity. However, both peptide ligands contain a C-terminal F8 that may be responsible for the "S"-shaped pose in their ligand binding pockets (39), and for activation of the receptors by triggering rotation of the "toggle switch" residue W$^{6.48}$. This action in turn facilitates the swing of F$^{6.44}$, initiating the outward movement of TM6. In these GPCRs, the hydrophobic core surrounding C terminus phenylalanine is composed of residues in TM2 (L/F$^{2.53}$), TM3 (L/M$^{3.36}$, L$^{3.32}$), TM6 (W$^{6.48}$, F/Y$^{6.51}$), and TM7 (Y/I$^{7.43}$) (40, 41). The binding pose of C9 is different from that of endogenous peptides like α-melanocyte-stimulating hormone (α-MSH), which lay flat at the extracellular face of melanocortin-1 receptor (MC1R) (42). The structural similarity between C9 binding and AngII binding raises the possibility that C9 (and chemerin) plays a role in vasoconstriction. It is notable that a recent study identified CMKLR1 expression in rat smooth muscle cells and endothelial cells, and C9 could contract human saphenous vein and resistance arteries (43). Whether CMKLR1 has functional features of the AT1 receptor remains to be investigated in future studies (40).

Wittamer et al. conducted a thorough investigation on the relationship between chemerin peptide length and composition and the induced cellular functions (17). Based on their study, the C-terminal nonapeptide has full agonistic activity, and extension of its N terminus did not add bioactivity. In contrast, the addition of an amino acid to its C terminus or removal of two amino acids from the C terminus reduced the potency of the peptide by three to four orders of magnitude. Their study also identified the essential elements of chemerin for full bioactivity in a nonapeptide, including Y1^{149}, G4^{152}, F6^{154}, F8^{156}, and S9^{157}, as their substitution by alanine led to decreases in bioactivity as well as binding by at least two orders of magnitudes (17). Our cryo-EM model provides a structural basis for the interaction of C9 with amino acids in the CMKLR1 binding pocket, and is consistent with the study of alanine-substituted C9 peptides.

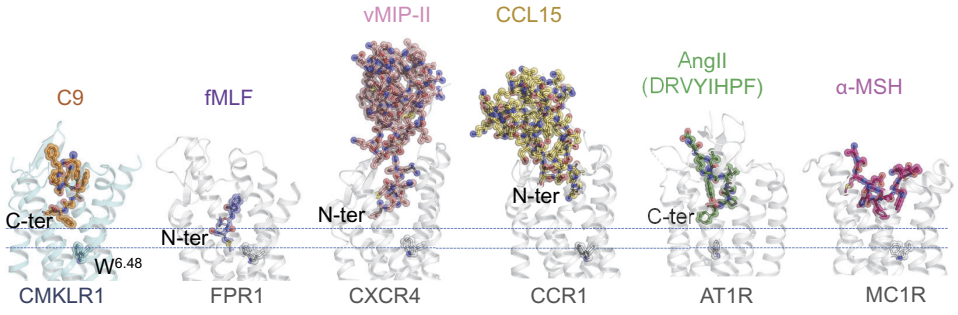

Fig. 5. Structural comparison of class A GPCRs activated by protein and peptide ligands. Structural comparison of ligand binding poses of selected GPCRs with their ligands, including (from *Left* to *Right*) CMKLR1 with C9 peptide, FPR1 with fMLF (PDB ID: 7EUO), CXCR4 with vMIP-II (PDB ID: 4RWS), CCR1 with CCL-15 (PDB ID: 7VLA), AngII in AT1R (PDB ID: 6OS0), and α-MSH in MC1R (PDB ID: 7F4D). The upper and lower dashed lines mark the positions of the ligand insertion bottom and W$^{6.48}$ in the receptor, respectively. The conserved residue W$^{6.48}$ in each receptor is shown in licorice and sphere and its position marked with a dashed line.

Our solved structure differs from a model proposed by Fischer et al., who used the Rosetta Suite for structure-based modeling of CMKLR1 interaction with the C9 peptide (44). In their predicted model, the C9 peptide assumes a "U-turn" pose with its G4 touching the bottom of the binding pocket and the remaining backbone of the C9 peptide turning upwards. The binding pocket is very shallow in this model, accommodating only four amino acids by depth. Moreover, the predicted model by Fischer et al. would place the critical $F8^{156}$ next to a hydrophobic pocket formed by ECL2, but this interaction could not explain why $F8^{156}$ is so critical to CMKLR1 activation. In contrast, our cryo-EM structure of CMKLR1 reveals that the peptide ligand folds into an "S" shape with its C-terminal F8 inserting deep into the binding pocket for activation of the receptor.

The cryo-EM structure of the C9-bound CMKLR1 provides useful information for comparative studies of this subgroup of Class A GPCRs that interact with small proteins and peptides. Of interest, C9 interaction with CMKLR1 differs from the two-site two-step binding mode of chemokine receptors, that involves an initial contact of the chemokine's N-loop/β3 region to the N-terminal region of the receptor before subsequent insertion of the N-terminal region of the chemokine into the binding pocket surrounded by the transmembrane helices for receptor activation (36, 45). The full agonist activity of C9 and its "S"-shaped pose in the binding pocket of CMKLR1 is akin to AngII in AT1 receptor, that provides a structural basis for newly identified functions of chemerin and its active peptides in the regulation of vasoconstriction and obesity-related metabolic disorders.

Materials and Methods

Expression Vector Design. For protein expression, the cDNAs encoding human CMKLR1, Human dominant negative Gαi1 (DNGαi1) with mutations (G203A/A326S), and scFv16 were cloned into the pFastBac vector (Thermo Fisher Scientific). The cDNAs for Gβ1 and Gγ2 were cloned into pFastBac-Dual vector (Thermo Fisher Scientific). For G protein dissociation assay and cAMP assay, the full-length CMKLR1 cDNAs with indicated point mutations were cloned into pcDNA3.1 vector (Thermo Fisher Scientific). For details, please refer to *SI Appendix, Materials and Methods*.

Expression and Purification of the CMKLR1-Gi Complexes. The CMKLR1, DNGαi1, Gβ1, and Gγ2 were coexpressed in Sf9 cells. After infection for 60 h, the cells were collected and lysed by lysis buffer containing the C9 peptide of chemerin. The CMKLR1-Gi complexes were then purified by anti-FLAG affinity resin and loaded onto the Fast Protein Liquid Chromatography (FPLC, ÄKTA™) system. Eluted fractions consisting of CMKLR1-Gi complexes were pooled and concentrated before being flash-frozen in liquid nitrogen and stored at −80 °C. These experiments are described in detail in *SI Appendix, Materials and Methods*.

Expression and Purification of scFv16. The scFv16 was expressed and secreted by *Trichoplusia ni* Hi5 insect cells. The supernatant was collected and purified by Ni-NTA resin. The flow-through was collected and loaded onto the ÄKTA FPLC system. Finally, the concentrated of scFv16 was flash frozen and stored in liquid nitrogen until further use. Detailed protocols are provided in *SI Appendix, Materials and Methods* sections.

Cryo-EM Sample Preparation and Data Collection. The purified C9-CMKLR1-Gi-scFv16 complex was spotted to the grid by adding to the glow-discharged amorphous alloy film. The complex was subsequently vitrified by plugging into liquid ethane using Vitrobot Mark IV (Thermo Fisher Scientific). Data collection was performed on a 300-kV Titan Krios Gi3 microscope (Thermo Fisher Scientific), at a magnification of 105,000 and a pixel size of 0.83 Å. Acquisition parameters are detailed in, *SI Appendix, Materials and Methods*.

Image Processing and Model Building. The image stacks were firstly subjected to patch motion correction and patch CTF estimation implemented in cryoSPARC 3.3.1 platform (Structura Biotechnology Inc.). After autopicking, the ab initio reconstruction was processed following 2D classification. A well-defined subset from heterogeneous refinements were subjected to non-uniform and local refinement for a map at 2.81 Å. The models were constructed using structure information from PDB ID code 7WXZ for portions of Gi1 and scFv16, and a predicted model from AlphaFold for portions of CMKLR1. The models were docked into the EM density map using UCSF Chimera version 1.12, followed by iterative manual building in Coot-0.9.2 and refinement in Phenix-1.18.2. The data collection and structure–refinement statistics are shown in *SI Appendix*, Table S1 and *Materials and Methods*.

Molecular Modeling and Molecular Dynamics Simulation. After adding the missing structure of the ECL2, the protonation state of the complete CMKLR1(30-328)-C9 complex was assigned by the web server H++ and charmm36m force field was employed in all simulations. After energy minimization, membrane relaxation and equilibrium simulation, five independent 1-μs-long production MD simulations were carried out for the CMKLR1-C9 complex. The parameters of MD simulation were described in *SI Appendix, Materials and Methods*.

G Protein Dissociation Assay. G protein activation was measured by a NanoBiT-based G protein dissociation assay. HEK 293T cells were transfected with CMKLR1, Gαi1-LgBiT, Gβ1, and SmBiT-Gγ2. After a one-day incubation, the cell suspension was seeded in a 384-well culture white plate and loaded with coelenterazine H solution. Then the CMKLR1 ligand was added to the cells and luminescence was measured by a Envision multimode plate reader. This experiment is described in detail in *SI Appendix, Materials and Methods*.

cAMP Assay. HEK 293T cells were transfected with CMKLR1 and FRET-based Epac sensors (mTurquoise2-Epac SH187-cp73venus-cp73venus). Forty-eight hours after transfection, the cells were treated with different concentrations of C9 peptide. Then forskolin were added and the intracellular cAMP level was measured with a FlexStation III microplate reader (Molecular Devices). For details, please refer to *SI Appendix, Materials and Methods* sections.

CMKLR1 Expression Level Determination by Flow Cytometry. HEK 293T cells were transfected with cDNA vectors for WT or mutant CMKLR1 for 24 h. The cells were then incubated with a human ChemR23 (CMKLR1) APC-conjugated antibody. The CMKLR1 expression level were quantified by flow cytometry. For experimental details, please refer to, *SI Appendix, Materials and Methods*.

Data, Materials, and Software Availability. The atomic coordinates for the model of C9-CMKLR1-Gi-scFv16 complex have been deposited to the Protein Data Bank (PDB) under the accession code 7YKD (46). The 3-dimentional cryo-EM density map has been deposited at the Electron Microscopy Data Bank under the accession number EMD-33891 (47). All study data are included in the article and/or *SI Appendix*.

ACKNOWLEDGMENTS. We thank the Kobilka Cryo-Electron Microscopy Center in the Chinese University of Hong Kong, Shenzhen for cryo-electron microscopy analysis. The computational work in this study was conducted on the High-Performance Computing Platform at The Chinese University of Hong Kong, Shenzhen. This work was supported in part by grants from the Shenzhen Natural Science Foundation GXWD20201231105722002-20200831175432002 (R.D.Y., Y.D. and L.Z.), Shenzhen Science and Technology Program JCYJ20200109150019113 (Y.D. and G.C.), Guangdong Basic and Applied Basic Research Foundation 2020A1515110726 (Q.L.) and 2020A1515111173 (G.C.), National Natural Science Foundation of China 82104183 (Q.L.) and 32070950 (R.D.Y.), the Ganghong Young Scholar Development Fund (R.D.Y.), and the Kobilka Institute of Innovative Drug Discovery at The Chinese University of Hong Kong, Shenzhen (Y.D. and R.D.Y.). The work was also supported by the Fellowship of China Postdoctoral Science Foundation 2021M703092 (J.W.), Presidential Fellowship of The Chinese University of Hong Kong, Shenzhen (Y.D. and R.D.Y.).

Author affiliations: [a]Kobilka Institute of Innovative Drug Discovery, School of Medicine, The Chinese University of Hong Kong, Shenzhen, Guangdong 518172, P.R. China; [b]Warshel Institute for Computational Biology, School of Medicine, The Chinese University of Hong Kong, Shenzhen, Guangdong 518172, P.R. China; and [c]Shenzhen Bay Laboratory, Shenzhen, Guangdong 518055, P.R. China

1. W. Meder *et al.*, Characterization of human circulating TIG2 as a ligand for the orphan receptor ChemR23. *FEBS Lett.* **555**, 495–499 (2003).
2. V. Wittamer *et al.*, Specific recruitment of antigen-presenting cells by chemerin, a novel processed ligand from human inflammatory fluids. *J. Exp. Med.* **198**, 977–985 (2003).
3. M. Samson *et al.*, ChemR23, a putative chemoattractant receptor, is expressed in monocyte-derived dendritic cells and macrophages and is a coreceptor for SIV and some primary HIV-1 strains. *Eur. J. Immunol.* **28**, 1689–1700 (1998).
4. B. A. Zabel, A. M. Silverio, E. C. Butcher, Chemokine-like receptor 1 expression and chemerin-directed chemotaxis distinguish plasmacytoid from myeloid dendritic cells in human blood. *J. Immunol.* **174**, 244–251 (2005).
5. B. A. Zabel *et al.*, Chemokine-like receptor 1 expression by macrophages in vivo: Regulation by TGF-beta and TLR ligands. *Exp. Hematol.* **34**, 1106–1114 (2006).
6. S. Parolini *et al.*, The role of chemerin in the colocalization of NK and dendritic cell subsets into inflamed tissues. *Blood* **109**, 3625–3632 (2007).
7. J. Weigert *et al.*, Systemic chemerin is related to inflammation rather than obesity in type 2 diabetes. *Clin. Endocrinol.* **72**, 342–348 (2010).
8. M. Lehrke *et al.*, Chemerin is associated with markers of inflammation and components of the metabolic syndrome but does not predict coronary atherosclerosis. *Eur. J. Endocrinol.* **161**, 339–344 (2009).
9. K. B. Goralski *et al.*, Chemerin, a novel adipokine that regulates adipogenesis and adipocyte metabolism. *J. Biol. Chem.* **282**, 28175–28188 (2007).
10. K. Bozaoglu *et al.*, Chemerin is a novel adipokine associated with obesity and metabolic syndrome. *Endocrinology* **148**, 4687–4694 (2007).
11. V. Catalan *et al.*, Increased levels of chemerin and its receptor, chemokine-like receptor-1, in obesity are related to inflammation: tumor necrosis factor-alpha stimulates mRNA levels of chemerin in visceral adipocytes from obese patients. *Surg. Obes. Relat. Dis.* **9**, 306–314 (2013).
12. Y. Lin *et al.*, The chemerin-CMKLR1 axis limits thermogenesis by controlling a beige adipocyte/IL-33/type 2 innate immunity circuit. *Sci. Immunol.* **6**, eabg9698 (2021).
13. Y. Lin *et al.*, Epithelial chemerin-CMKLR1 signaling restricts microbiota-driven colonic neutrophilia and tumorigenesis by up-regulating lactoperoxidase. *Proc. Natl. Acad. Sci. U.S.A.* **119**, e2205574119 (2022).
14. M. C. Miller, K. H. Mayo, Chemokines from a structural perspective. *Int. J. Mol. Sci.* **18**, 2088 (2017).
15. M. C. Ernst, C. J. Sinal, Chemerin: At the crossroads of inflammation and obesity. *Trends Endocrinol. Metab.* **21**, 660–667 (2010).
16. B. A. Zabel *et al.*, Chemerin activation by serine proteases of the coagulation, fibrinolytic, and inflammatory cascades. *J. Biol. Chem.* **280**, 34661–34666 (2005).
17. V. Wittamer *et al.*, The C-terminal nonapeptide of mature chemerin activates the chemerin receptor with low nanomolar potency. *J. Biol. Chem.* **279**, 9956–9962 (2004).
18. I. Gantz *et al.*, Molecular cloning of a novel receptor (CMKLR1) with homology to the chemotactic factor receptors. *Cytogenet. Cell Genet.* **74**, 286–290 (1996).
19. J. Kaur, R. Adya, B. K. Tan, J. Chen, H. S. Randeva, Identification of chemerin receptor (ChemR23) in human endothelial cells: Chemerin-induced endothelial angiogenesis. *Biochem. Biophys. Res. Commun.* **391**, 1762–1768 (2010).
20. K. J. Ho *et al.*, Aspirin-triggered lipoxin and resolvin E1 modulate vascular smooth muscle phenotype and correlate with peripheral atherosclerosis. *Am. J. Pathol.* **177**, 2116–2123 (2010).
21. A. Marchese *et al.*, Cloning of human genes encoding novel G protein-coupled receptors. *Genomics* **23**, 609–618 (1994).
22. G. Barnea *et al.*, The genetic design of signaling cascades to record receptor activation. *Proc. Natl. Acad. Sci. U.S.A.* **105**, 64–69 (2008).
23. A. J. Kennedy, A. P. Davenport, International Union of Basic and Clinical Pharmacology CIII: Chemerin receptors CMKLR1 (Chemerin1) and GPR1 (Chemerin2) nomenclature, pharmacology, and function. *Pharmacol. Rev.* **70**, 174–196 (2018).
24. S. Maeda *et al.*, Development of an antibody fragment that stabilizes GPCR/G-protein complexes. *Nat. Commun.* **9**, 3712 (2018).
25. J. A. Ballesteros, H. Weinstein, "[19] Integrated methods for the construction of three-dimensional models and computational probing of structure-function relations in G protein-coupled receptors" in *Methods in Neurosciences*, (Elsevier, 1995), **vol. 25**, pp. 366–428.
26. Y. Zhu *et al.*, Structural basis of FPR2 in recognition of Abeta42 and neuroprotection by humanin. *Nat. Commun.* **13**, 1775 (2022).
27. Y. Zhuang *et al.*, Molecular recognition of formylpeptides and diverse agonists by the formylpeptide receptors FPR1 and FPR2. *Nat. Commun.* **13**, 1054 (2022).
28. Y. Zhuang *et al.*, Structure of formylpeptide receptor 2-Gi complex reveals insights into ligand recognition and signaling. *Nat. Commun.* **11**, 885 (2020).
29. T. Chen *et al.*, Structural basis of ligand binding modes at the human formyl peptide receptor 2. *Nat. Commun.* **11**, 1208 (2020).
30. Q. Zhou *et al.*, Common activation mechanism of class A GPCRs. *Elife* **8**, e50279 (2019).
31. W. I. Weis, B. K. Kobilka, The molecular basis of G protein-coupled receptor activation. *Annu. Rev. Biochem.* **87**, 897–919 (2018).
32. O. De Henau *et al.*, Signaling properties of chemerin receptors CMKLR1, GPR1 and CCRL2. *PLoS One* **11**, e0164179 (2016).
33. E. Lee, R. Taussig, A. G. Gilman, The G226A mutant of Gs alpha highlights the requirement for dissociation of G protein subunits. *J. Biol. Chem.* **267**, 1212–1218 (1992).
34. B. A. Posner, M. B. Mixon, M. A. Wall, S. R. Sprang, A. G. Gilman, The A326S mutant of Giα1 as an approximation of the receptor-bound state. *J. Biol. Chem.* **273**, 21752–21758 (1998).
35. J. P. Mahoney, R. K. Sunahara, Mechanistic insights into GPCR-G protein interactions. *Curr. Opin. Struct. Biol.* **41**, 247–254 (2016).
36. M. M. Rosenkilde, N. Tsutsumi, J. M. Knerr, D. F. Kildedal, K. C. Garcia, Viral G protein-coupled receptors encoded by beta- and gamma-Herpesviruses. *Annu. Rev. Virol.* **9**, 329–351 (2022), 10.1146/annurev-virology-100220-113942.
37. Z. Shao *et al.*, Identification and mechanism of G protein-biased ligands for chemokine receptor CCR1. *Nat. Chem. Biol.* **18**, 264–271 (2022).
38. R. D. Ye *et al.*, International Union of Basic and Clinical Pharmacology. LXXIII. Nomenclature for the formyl peptide receptor (FPR) family. *Pharmacol. Rev.* **61**, 119–161 (2009).
39. L. M. Wingler *et al.*, Angiotensin and biased analogs induce structurally distinct active conformations within a GPCR. *Science* **367**, 888–892 (2020).
40. L. M. Wingler, R. J. Lefkowitz, Conformational basis of G protein-coupled receptor signaling versatility. *Trends Cell Biol.* **30**, 736–747 (2020).
41. C. M. Suomivuori *et al.*, Molecular mechanism of biased signaling in a prototypical G protein-coupled receptor. *Science* **367**, 881–887 (2020).
42. S. Ma *et al.*, Structural mechanism of calcium-mediated hormone recognition and Gβ interaction by the human melanocortin-1 receptor. *Cell Res.* **31**, 1061–1071 (2021).
43. A. J. Kennedy *et al.*, Chemerin elicits potent constrictor actions via chemokine-like receptor 1 (CMKLR1), not G-protein-coupled receptor 1 (GPR1), in human and rat vasculature. *J. Am. Heart Assoc.* **5**, e004421 (2016).
44. T. F. Fischer *et al.*, Cyclic analogues of the chemerin C-terminus mimic a loop conformation essential for activating the chemokine-like receptor 1. *J. Med. Chem.* **64**, 3048–3058 (2021).
45. J. Sanchez *et al.*, Evaluation and extension of the two-site, two-step model for binding and activation of the chemokine receptor CCR1. *J. Biol. Chem.* **294**, 3464–3475 (2019).
46. G. Chen, Q. Liao, J. Wang,R. D. Ye , Cryo-EM structure of the human chemerin receptor 1 complex with the C-terminal nonapeptide of chemerin. *Protein Data Bank*. https://www.rcsb.org/structure/7YKD. Deposited July 22, 2022.
47. G. Chen, Q. Liao, J. Wang,R. D. Ye, Cryo-EM structure of the human chemerin receptor 1 complex with the C-terminal nonapeptide of chemerin. *Electron Microscopy Data Bank*. https://www.ebi.ac.uk/emdb/EMD-33891. Deposited July 22, 2022.